Editors' Suggestion

Germanium Vacancy in Diamond Quantum Memory Exceeding 20 ms

Katharina Senkalla,[1,*] Genko Genov,[1] Mathias H. Metsch,[1] Petr Siyushev,[1,2,3] and Fedor Jelezko[1]
[1]Institute for Quantum Optics, Ulm University, Albert-Einstein-Allee 11, 89081 Ulm, Germany
[2]3rd Institute of Physics, Center for Applied Quantum Technologies University of Stuttgart, Stuttgart, Germany
[3]Institute for Materials Research (IMO), Hasselt University, Wetenschapspark 1, B-3590 Diepenbeek, Belgium

(Received 27 July 2023; accepted 29 November 2023; published 11 January 2024)

Negatively charged group-IV defects in diamond show great potential as quantum network nodes due to their efficient spin-photon interface. However, reaching sufficiently long coherence times remains a challenge. In this work, we demonstrate coherent control of germanium vacancy center (GeV) at millikelvin temperatures and extend its coherence time by several orders of magnitude to more than 20 ms. We model the magnetic and amplitude noise as an Ornstein-Uhlenbeck process, reproducing the experimental results well. The utilized method paves the way to optimized coherence times of group-IV defects in various experimental conditions and their successful applications in quantum technologies.

DOI: 10.1103/PhysRevLett.132.026901

Quantum networks have the potential to enhance the way we communicate and process information by enabling new technologies such as distributed quantum computing, enhanced sensing, and secure quantum communication [1–5]. Specifically, long-distance quantum communication remains an open challenge, as it requires qubits that act as a long-lived quantum memory for efficient entanglement distribution.

Recent studies have reported the great potential of negatively charged group-IV defects in diamond as a quantum network node [6,7]. The defects share outstanding optical properties such as high flux of coherent photons (Debye-Waller factor up to ∼70%), Fourier-transform-limited optical transitions, and exceptional spectral stability imposed by the inversion symmetry of the defect's structure [6]. Spectral stability is essential for the integration into nanophotonic devices, which has already been demonstrated for various defects [8–10]. In order to satisfy all requirements for a network node, the systems should, moreover, provide access to a well-controllable spin qubit with a long quantum memory time. Such control has been demonstrated with silicon-vacancy centers (SiV) in diamond, with memory times approaching ∼10 ms [11]. Despite the showcased achievements, the SiV's electron spin suffers of phonon-mediated decoherence due to its small orbital ground state splitting (48 GHz), as shown in [12,13]. To mitigate this effect, approaches such as strain engineering of the defects [14,15] or operation in dilution refrigerators [11,16] have been explored. Strain may potentially impact the spectral stability of the defect and introduce additional complexity, so operating at low temperatures remains the preferred solution. However, performing experiments in dilution refrigerators requires a careful adjustment of the induced heat load as the cooling power is limited.

These challenges have motivated efforts for the investigation of other group-IV defects. These defects provide not only enhanced optical properties, such as higher coherent flux of photons, but also an increasing spin-orbit splitting across the group, which allows operation at elevated temperatures [6,7]. The germanium vacancy (GeV) is considered as a promising alternative. The fabrication is relatively easy [9,17], similarly to SiV, preserving good optical characteristics. However, the suppression of phonon relaxation at a few hundred millikelvin is more than four orders of magnitude higher compared to SiV. This enables the use of strong microwave (MW) fields for coherent control.

In this Letter, we demonstrate for the first time efficient initialization, readout, and coherent control of a negatively charged GeV center at temperatures below 300 mK. At these temperatures, the phonon relaxation process is suppressed, and we observe spin noise limited coherence time of the order of $T_2^* \approx 1.43$ μs. We prolong the quantum memory time by several orders of magnitude to more than 20 ms by dynamical decoupling (DD) protocols. The achieved memory time exceeds the one of SiV by a factor of two [11], demonstrating that GeV is a viable alternative for quantum memory applications. Our analysis shows that magnetic noise due to interactions with the spin environment and power fluctuations of the driving field can account for the most of the observed decoherence. The noise is modeled as an Ornstein-Uhlenbeck process [18], resulting in good agreement of the simulations and the experimental results. These findings allow for the design of efficient control strategies for extending the coherence times even further, e.g., by using higher-order DD sequences and tailoring the interpulse time separation [19–21]. The demonstration of efficient initialization, readout, and coherent control in combination with long memory times of

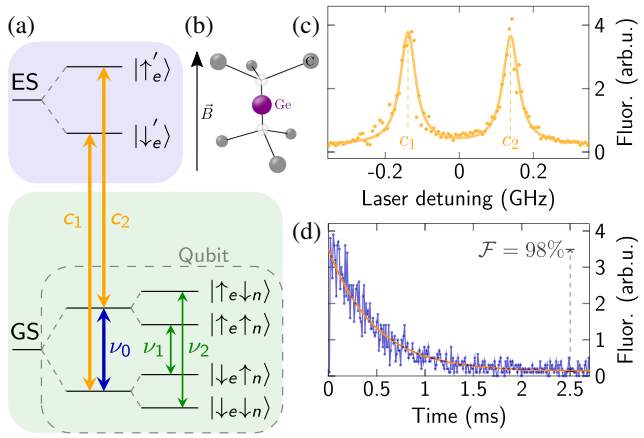

FIG. 1. (a) Reduced energy level scheme showing the lower orbital branches in the ground (green) and excited (blue) state manifold. The electron spin becomes accessible by applying an external magnetic field $B = 100$ mT (b) through the optical transitions $c_{1,2}$. (c) Corresponding PLE spectrum under constant MW repumping at frequency ν_0. Slight misalignment of $\vec{B}$ to the GeV axis allows for efficient optical initialization of 98% within 1 ms (d).

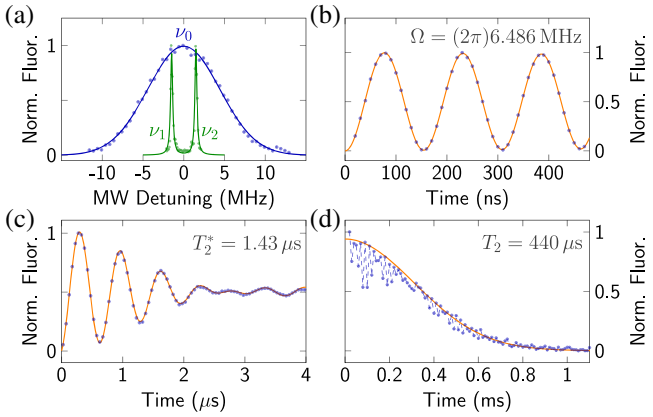

FIG. 2. (a) ODMR spectrum (shown in green) shows transition frequencies $\nu_{1,2}$ with 300 kHz linewidth. The separation by 2.98 MHz indicates a strongly coupled ^{13}C. For further measurement, the driving field $\nu_0 = 3.066$ GHz was chosen such that both transitions are equally covered (shown in blue). (b) Corresponding Rabi oscillations with a frequency of $\Omega = (2\pi)6.486$ MHz. (c) Ramsey interference measurement reveals $T_2^* = 1.43$ μs. (d) Hahn echo decay measurement yields spin-noise-limited $T_2 = 440$ μs.

negatively charged GeV centers opens the door for multiple quantum technology applications, e.g., in quantum communication and quantum information.

Experimental setup and results.—We perform the experiments on a $\langle 1,1,1\rangle$-oriented synthetic diamond grown via high-pressure high-temperature method with Ge incorporation during this process [22]. During this high-pressure high-temperature growth process, germanium (Ge) is naturally incorporated into the diamond, leading to the formation of GeV without requiring any additional treatments. To optimize the collection efficiency, we fabricate a solid immersion lens with 10 μm diameter into the diamond and position a 20-μm-thick wire nearby which delivers the microwave field. The sample is mounted on a cold finger of an optical dilution refrigerator combined with a home-built confocal microscope for individual addressing of GeV centers. The superconducting vector magnet allows for arbitrary alignment of a magnetic field with respect to the principal axis of the defect. Further details about the device preparation can be found in [23].

Figure 1(a) shows a reduced energy level diagram of the GeV center, emphasizing the relevant sublevels for the spin dynamics. At temperatures $T < (h\Delta_g/k_B)$, with h as Planck's constant, Δ_g as ground state splitting, and k_B as the Boltzmann constant, the orbital relaxation process becomes exponentially suppressed. We maintain a temperature below 300 mK in all experiments [23], so we consider only the lower orbital branches of the ground state (GS) and excited state (ES) manifold. To access the spin degree of freedom, we apply a magnetic field $B = 100$ mT and exploit the difference of the Zeeman splitting in GS and ES for resonant optical addressing. Figure 1(c) shows the photoluminescence excitation (PLE) spectrum of the optical transitions $c_{1,2}$ in Fig. 1(a) using an optical power of 2 nW directed into the cryostat. Their spin-conserving nature leads to long cyclicity and, thus, to a low spin polarization rate. We choose a slightly misaligned magnetic field to induce spin state mixing, which reduces the required optical pumping time to 1 ms with 98% initialization fidelity. Figure 1(d) shows the corresponding time-dependent luminescence trace using transition c_2. The fully initialized spin cannot be further driven by a field with frequency c_2 and, thus, is referred to as the "dark state." As in the millikelvin environment relaxation processes of the electron spin do not occur on relevant timescales [11,16], a repumping scheme is required to resolve both transitions in PLE measurements. This can be achieved either by using an additional pump laser [16] or by resonantly flipping the spin using microwave control.

We determine the resonance frequency ν_0 by sweeping a microwave around 3 GHz after initialization in the dark state. When the MW frequency matches the Zeeman splitting between the ground states, the population and, thus, the fluorescence are restored, leading to an optically detectable magnetic resonance (ODMR). We note that, within one orbital branch, the orbital states are orthogonal which would, in principle, prevent direct microwave driving. However, the GeV center under investigation shows a signature of strain with $\Delta_g = 181$ GHz [23], so the orbital states mix and the transitions become allowed. We refer to Fig. S6 in [23] for an extended level scheme and corresponding PLE measurements.

The ODMR results shown in Fig. 2(a) are conducted in a pulsed manner [27]. We observe a splitting of 2.98 MHz due to hyperfine coupling to a nearby ^{13}C nuclear spin with

the linewidths of ν_1 and ν_2 approximately 300 kHz [green curve in Fig. 2(a)]. We set the frequency of the driving field to $\nu_0 = 3.066$ GHz for the further measurements, so it covers equally well both transitions $\nu_{1,2}$ due to power broadening [Fig. 2(a), blue curve]. We observe Rabi oscillations in Fig. 2(b) and estimate a Rabi frequency of $\Omega = (2\pi)6.486$ MHz at 36 dBm input power into the cryostat, inferring a π pulse duration of 77.09 ns. At the start of each experiment, the system is initialized in the dark state and subsequently coherently controlled using rectangular π and $(\pi/2)$ pulses with durations determined from the Rabi measurement.

We investigate the electron coherence time utilizing Ramsey interferometry, consisting of two $(\pi/2)$ pulses and a variable interpulse delay. This and all following measurements are performed in an alternating manner where we change the phase of the latter $(\pi/2)$ pulse between X (0°) and $-X$ (180°) to project onto the dark and bright states. We consider then the differential signal between them to reduce the effect of laser fluctuations and normalize to the maximum fluorescence difference unless otherwise stated [23]. By fitting the spin decay in Fig. 2(c), we find the inhomogeneous spin dephasing time of $T_2^* \approx 1.43$ μs. The oscillatory signal arises due to the microwave frequency detuning from the transitions $\nu_{1,2}$ to ν_0, confirming the hyperfine coupling of 2.98 MHz.

By operating in a temperature regime in which the phonon-induced transitions between orbital states are suppressed, the dephasing is mainly caused by magnetic noise. For this regime, the coherence time T_2 can be significantly extended compared to T_2^* using dynamical decoupling (DD) protocols. These include π pulses that periodically aim to refocus the phase accumulated by the GeV center due to interactions with the surrounding nuclear and electron spin bath [28]. The Hahn echo is the simplest DD protocol having one additional π pulse in the free evolution time between the two $(\pi/2)$ pulses of the Ramsey experiment. Figure 2(d) shows the corresponding decay curve, which exhibits a modulation that can be attributed to the entangling and disentangling to the ^{13}C spin bath. However, the modulation contrast is low due to the high Larmor precession frequency (≈1.03 MHz [23]) and the undersampling of the pulse separation τ. From the fit we extract the spin coherence time $T_2 \approx 440$ μs. This timescale is consistent with the theoretically predicted hyperfine noise limit for diamonds with natural abundance of ^{13}C [29].

The coherence time can be further extended using DD with multiple refocusing pulses [28,30]. First, we apply the Carr-Purcell-Meiboom-Gill (CPMG) sequence consisting of an even number of π pulses shifted by 90° with respect to the $(\pi/2)$ pulses [Fig. 3(a)] [31,32]. In a first series of DD measurements, we keep the number of repetition pulses N constant while sweeping the interpulse delays τ. Figure 3(b) illustrates the extension of the coherence time

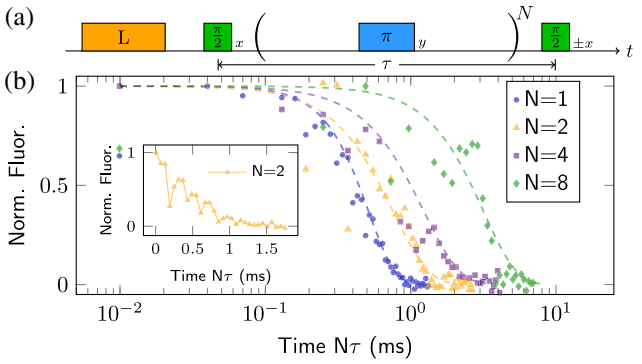

FIG. 3. (a) CPMG sequence with N refocusing π pulses separated by τ. The phase of each pulse is indicated in a subscript. (b) Decay curves with fixed $N = \{1, 2, 4, 8\}$ and increasing τ. Dashed lines show fits of the envelopes to $\exp[-(N\tau/T_2)^\beta]$ with β a free parameter. Inset: Enlargement of $N = 2$ measurement, showing regular dips due to entangling and disentangling to a ^{13}C.

with increasing N. The signal shows pronounced dips due to coupling to ^{13}C, as exemplary shown for $N = 2$ in the inset in Fig. 3(b). Fitting the various datasets to a stretched exponential exhibits memory times up to 7 times longer than for the Hahn echo.

Experiments where the interpulse delay τ is varied and the number of pulses N is kept constant are typically used to probe the spin environment noise spectrum [33]. However, in quantum memory experiments, we usually choose an optimal interpulse delay τ and vary the number of pulses N [19–21,34–37]. This allows for memory time optimization and readout at arbitrary times when the quantum state is refocused. To explore the limit of the spin memory time, we thus vary the order N for the CPMG and $XY8$ sequences [Fig. 4(a)], keeping constant a pulse spacing of $\tau = 100$ μs for which the Hahn echo decay is negligible. We note that the pulse separation can be optimized further by tailoring it to the specific DD sequence [21] and by avoiding unwanted coupling to the ^{13}C bath, e.g., due to spurious harmonics [38]. We choose the CPMG and $XY8$ sequences because the former is highly robust to errors when the initial $\pi/2$ pulse is shifted by 90° with respect to the subsequent π pulses. However, its fidelity suffers if the initial $\pi/2$ pulse has the same phase [23,31,32,34,39]. We thus also apply the widely used $XY8$ sequence, consisting of eight consecutive π pulses, with phases of 0° (X) and 90° (Y), as depicted in Fig. 4(c). It is robust to pulse errors and has a high fidelity for unknown initial states [34,39,40]. A discussion on the fidelities of the pulses, CPMG and $XY8$, is included in [23]. We note that even more advanced sequences can be applied like the Knill dynamical decoupling sequence [34] or a sequence from the universally robust family [20,21], which could, in principle, achieve even longer memory times.

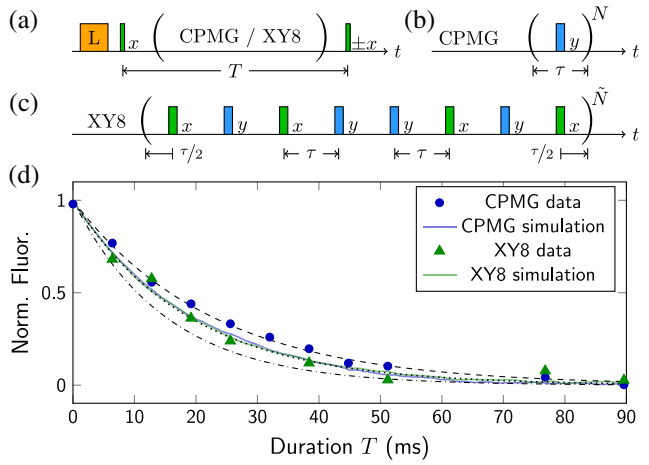

FIG. 4. (a) Memory measurement sequence using the CPMG (b) and $XY8$ (c) protocol. Subscripts represent the phase of a pulse. (d) Experimental results for CPMG (blue dots) and $XY8$ (green triangles) with fixed $\tau = 100$ μs and sweeping order N, $\tilde{N}$ vs the total duration time T. Fluorescence is normalized to the expected value for $T = 0$ for each sequence [23]. Exponential decay fitting yields $T_{2,\mathrm{CPMG}} = 24.1 \pm 0.9$ ms and $T_{2,XY8} = 18 \pm 3$ ms. Solid lines represent OU simulations for CPMG (blue) and $XY8$ (green), closely matching the measured data. The results remain within the simulation curves for the boundaries of the correlation time of 12.4 s (18.6 s), displayed as dashed (dash-dotted) lines (see the text and [23]).

Figure 4 shows the measurement sequences [Figs. 4(a)–4(c)] and the corresponding decay curves [Fig. 4(d)], where we progressively increase the memory time by changing the order N or $\tilde{N} = N/8$ (for $XY8$) while keeping τ constant. A simple exponential fit to the data yields $T_{2,\mathrm{CPMG}} = 24.1 \pm 0.9$ ms and $T_{2,XY8} = 18 \pm 3$ ms [23]. Compared to the Hahn echo T_2, this is a 45-fold (CPMG) and 40-fold ($XY8$) extension, respectively.

Noise model and numerical simulation.—In order to characterize the performance of the DD sequences and possibly prolong the coherence time, we perform numerical simulations of decoherence during DD. For this purpose, we consider a simplified model of a two-state quantum system, which is subject to magnetic noise and power fluctuations of the driving fields. The decoherence model is similar to the one used in other color centers in diamond, e.g., NV centers [41–44]. It assumes that resonant interactions (flip flops) between the GeV and the bath spins (apart from ^{13}C) are negligible due to a large energy mismatch. Thus, the effect of the bath is dephasing of the GeV spin and can be approximated by magnetic noise along the GeV's quantization axis. In order to analyze decoherence during DD, we consider the Hamiltonian in the rotating frame at the carrier frequency ω of the pulses after applying the rotating-wave approximation ($\Omega \ll \omega$) [23]:

$$H_1(t) = \frac{\delta(t)}{2}\sigma_z + \frac{\tilde{\Omega}(t)}{2}\{\cos[\phi(t)]\sigma_x + \sin[\phi(t)]\sigma_y\}, \quad (1)$$

where $\tilde{\Omega}(t) = \Omega[1 + \epsilon(t)]f(t)$ is the magnitude of the Rabi frequency with $\Omega = (2\pi)\,6.486$ MHz its target peak value, $f(t)$ describes its expected time dependence (e.g., it can be 0 or 1), $\epsilon(t)$ characterizes the amplitude noise, and $\phi(t)$ is its relative phase (e.g., 0° or 90°). The detuning $\delta(t)$ is the difference in the Larmor frequency of the GeV electron spin from the angular frequency of the driving field ω, e.g., due to the hyperfine splitting and magnetic noise. Similarly to other experiments in color centers in diamond [41–44], we model $\delta(t)$ with an Ornstein-Uhlenbeck (OU) process [45,46] with a zero expectation value $\langle\delta(t)\rangle = 0$ and correlation function $\langle\delta(t)\delta(t')\rangle = \sigma_\delta^2 \exp(-\gamma|t - t'|)$, where $\sigma_\delta^2 = \langle\delta(t)^2\rangle$ is the variance of the detuning due to noise, $\sigma_\delta \approx \sqrt{2}/T_2^* \approx (2\pi)\,146$ kHz [23,35,41,46], with $T_2^* \approx 1.43$ μs the decay time of the signal from the Ramsey measurement in Fig. 2(c). We fit the decay shape of the signal from the CPMG and $XY8$ experiments and obtain an estimate of the correlation time $\tau_c = 1/\gamma$ in the range of 12.4 and 18.7 s with an expected value of $\tau_c \approx 15.5$ s [23]. The variation in the estimated values is likely due to fit uncertainty and slight changes in magnetic noise during operation, e.g., due to drift in temperature or alignment. We plot the theoretical coherence decay curves for DD with ideal, instantaneous π pulses for an OU process [23,35] for the expected $\tau_c = 15.5$ s (dotted line) and the upper (lower) values of the estimated range $\tau_c = 18.7$ s ($\tau_c = 12.4$ s) as dashed (dashed-dotted) lines in Fig. 4(d).

The amplitude error $\epsilon(t)$ is also modeled by an OU process with standard deviation $\sigma_\epsilon = 0.005$ and correlation time $\tau_\Omega = 500$ μs, similarly to previous work [23,42]. We calculate the $\delta(t)$ and $\epsilon(t)$ for 2500 different noise realizations, simulate the evolution of the system for each, and obtain the average the density matrix from all noise realizations. The simulated signal decay [23] is shown as solid blue (CPMG) and solid green ($XY8$) lines in Fig. 4(d), resulting in simulation estimates for the coherence times of $T_{2,\mathrm{CPMG}} = 19.8$ ms and $T_{2,XY8} = 19.2$ ms [23]. The experimental data fit well to the simulation results, especially for $XY8$, while the CPMG data also lie within the expected range of the theoretical decay curves for the noise model. The good fit of the experimental data, simulation results, and theoretical decay curves indicate excellent control of the system and compensation of experimental imperfections. CPMG slightly outperforms $XY8$, most likely due to the effect of spin locking and possibly a nonzero interaction of the GeV electron spin with the strongly coupled ^{13}C for $XY8$ at $\tau = 100$ μs [23], which is not considered in the simulations. The good agreement between experiment and simulation confirms the OU process as a valid way to model the environmental noise and field errors, identifying them as the main limit for the coherence time. The noise

model can also be applicable to other color centers in diamond, e.g., SiV centers [11], to enhance the understanding of decoherence for group-IV defects. This, in principle, allows for the design of optimized control sequences to prolong the coherence time further, e.g., by carefully choosing the interpulse delay or using higher-order DD [19–21].

Conclusion.—We demonstrated for the first time efficient initialization, readout, and coherent control of the electron spin of the GeV at millikelvin temperatures. We applied dynamical decoupling sequences and increased the coherence time by several orders of magnitude to more than 20 ms, which is the longest coherence time for group-IV defects up to date, to the best of our knowledge. The performed decoherence simulations fit the experimental data reasonably well, validating the noise model and allowing for the design of optimized control schemes for GeV and other group-IV defects. Using isotopically enriched ^{12}C diamonds could allow for even longer memory times. Another strategy to enhance memory time involves storing the quantum state in long-lived nuclear spins, either those inherent to GeV itself [47] or the neighboring ^{13}C spins through dynamical decoupling applied to the GeV electron spin [48–50]. The results demonstrate the applicability of the GeV as a quantum memory, overcoming one main obstacle for quantum technology applications of group-IV defects, e.g., for quantum communication.

We thank Yuri N. Palyanov, Igor N. Kupriyanov, and Yuri M. Borzdov for providing the sample used in this work. This work was supported by Deutsche Forschungsgemeinschaft (DFG) via Projects No. 386028944, No. 445243414, and No. 387073854, H2020 European Research Council (ERC) Synergy grant HyperQ (Grant No. 856432), Baden-Württemberg Stiftung and Volkswagen Stiftung, Bundesministerium für Bildung und Forschung (BMBF) via project QuMicro, SPINNING, CoGeQ, QR.X, and Quantum HiFi.

*Corresponding author: katharina.senkalla@uni-ulm.de

[1] H. J. Kimble, The quantum internet, Nature (London) **453**, 1023 (2008).
[2] L. I. Childress, J. M. Taylor, A. Sørensen, and M. D. Lukin, Fault-tolerant quantum repeaters with minimal physical resources and implementations based on single-photon emitters, Phys. Rev. A **72**, 052330 (2005).
[3] D. Gottesman, T. Jennewein, and S. Croke, Longer-baseline telescopes using quantum repeaters, Phys. Rev. Lett. **109**, 070503 (2012).
[4] P. Komar, E. M. Kessler, M. Bishof, L. Jiang, A. S. Sørensen, J. Ye, and M. D. Lukin, A quantum network of clocks, Nat. Phys. **10**, 582 (2014).
[5] C. Monroe, R. Raussendorf, A. Ruthven, K. R. Brown, P. Maunz, L.-M. Duan, and J. Kim, Large-scale modular quantum-computer architecture with atomic memory and photonic interconnects, Phys. Rev. A **89**, 022317 (2014).
[6] C. Bradac, W. Gao, J. Forneris, M. E. Trusheim, and I. Aharonovich, Quantum nanophotonics with group IV defects in diamond, Nat. Commun. **10**, 5625 (2019).
[7] M. Ruf, N. H. Wan, H. Choi, D. Englund, and R. Hanson, Quantum networks based on color centers in diamond, J. Appl. Phys. **130**, 070901 (2021).
[8] A. Sipahigil, R. E. Evans, D. D. Sukachev, M. J. Burek, J. Borregaard, M. K. Bhaskar, C. T. Nguyen, J. L. Pacheco, H. A. Atikian, C. Meuwly, R. M. Camacho, F. Jelezko, E. Bielejec, H. Park, M. Lončar, and M. D. Lukin, An integrated diamond nanophotonics platform for quantum-optical networks, Science **354**, 847 (2016).
[9] M. K. Bhaskar, D. D. Sukachev, A. Sipahigil, R. E. Evans, M. J. Burek, C. T. Nguyen, L. J. Rogers, P. Siyushev, M. H. Metsch, H. Park *et al.*, Quantum nonlinear optics with a germanium-vacancy color center in a nanoscale diamond waveguide, Phys. Rev. Lett. **118**, 223603 (2017).
[10] A. E. Rugar, C. Dory, S. Aghaeimeibodi, H. Lu, S. Sun, S. D. Mishra, Z.-X. Shen, N. A. Melosh, and J. Vučković, Narrow-linewidth tin-vacancy centers in a diamond waveguide, ACS Photonics **7**, 2356 (2020).
[11] D. D. Sukachev, A. Sipahigil, C. T. Nguyen, M. K. Bhaskar, R. E. Evans, F. Jelezko, and M. D. Lukin, Silicon-vacancy spin qubit in diamond: A quantum memory exceeding 10 ms with single-shot state readout, Phys. Rev. Lett. **119**, 223602 (2017).
[12] K. D. Jahnke, A. Sipahigil, J. M. Binder, M. W. Doherty, M. Metsch, L. J. Rogers, N. B. Manson, M. D. Lukin, and F. Jelezko, Electron–phonon processes of the silicon-vacancy centre in diamond, New J. Phys. **17**, 043011 (2015).
[13] B. Pingault, D.-D. Jarausch, C. Hepp, L. Klintberg, J. N. Becker, M. Markham, C. Becher, and M. Atatüre, Coherent control of the silicon-vacancy spin in diamond, Nat. Commun. **8**, 15579 (2017).
[14] S. Meesala, Y.-I. Sohn, B. Pingault, L. Shao, H. A. Atikian, J. Holzgrafe, M. Gündoğan, C. Stavrakas, A. Sipahigil, C. Chia, R. Evans, M. J. Burek, M. Zhang, L. Wu, J. L. Pacheco, J. Abraham, E. Bielejec, M. D. Lukin, M. Atatüre, and M. Lončar, Strain engineering of the silicon-vacancy center in diamond, Phys. Rev. B **97**, 205444 (2018).
[15] P.-J. Stas, Y. Q. Huan, B. Machielse, E. N. Knall, A. Suleymanzade, B. Pingault, M. Sutula, S. W. Ding, C. M. Knaut, D. R. Assumpcao, Y.-C. Wei, M. K. Bhaskar, R. Riedinger, D. D. Sukachev, H. Park, M. Lončar, D. S. Levonian, and M. D. Lukin, Robust multi-qubit quantum network node with integrated error detection, Science **378**, 557 (2022).
[16] J. N. Becker, B. Pingault, D. Groß, M. Gündoğan, N. Kukharchyk, M. Markham, A. Edmonds, M. Atatüre, P. Bushev, and C. Becher, All-optical control of the silicon-vacancy spin in diamond at millikelvin temperatures, Phys. Rev. Lett. **120**, 053603 (2018).
[17] P. Siyushev, M. H. Metsch, A. Ijaz, J. M. Binder, M. K. Bhaskar, D. D. Sukachev, A. Sipahigil, R. E. Evans, C. T. Nguyen, M. D. Lukin, P. R. Hemmer, Y. N. Palyanov, I. N. Kupriyanov, Y. M. Borzdov, L. J. Rogers, and F. Jelezko,

Optical and microwave control of germanium-vacancy center spins in diamond, Phys. Rev. B **96**, 081201(R) (2017).
[18] D. T. Gillespie, Exact numerical simulation of the Ornstein-Uhlenbeck process and its integral, Phys. Rev. E **54**, 2084 (1996).
[19] A. Ajoy, G. A. Álvarez, and D. Suter, Optimal pulse spacing for dynamical decoupling in the presence of a purely dephasing spin bath, Phys. Rev. A **83**, 032303 (2011).
[20] G. T. Genov, D. Schraft, N. V. Vitanov, and T. Halfmann, Arbitrarily accurate pulse sequences for robust dynamical decoupling, Phys. Rev. Lett. **118**, 133202 (2017).
[21] N. Ezzell, B. Pokharel, L. Tewala, G. Quiroz, and D. A. Lidar, Dynamical decoupling for superconducting qubits: A performance survey, arXiv:2207.03670.
[22] Y. N. Palyanov, I. N. Kupriyanov, Y. M. Borzdov, and N. V. Surovtsev, Germanium: A new catalyst for diamond synthesis and a new optically active impurity in diamond, Sci. Rep. **5**, 14789 (2015).
[23] See Supplemental Material at http://link.aps.org/supplemental/10.1103/PhysRevLett.132.026901 for the numerical simulation, noise calibration, experimental setup, GeV physical system, and details on quantum memory time experiments with Refs. [24–26] included therein.
[24] N. Aharon, I. Schwartz, and A. Retzker, Quantum control and sensing of nuclear spins by electron spins under power limitations, Phys. Rev. Lett. **122**, 120403 (2019).
[25] G. E. Santyr, R. M. Henkelman, and M. J. Bronskill, Variation in measured transverse relaxation in tissue resulting from spin locking with the CPMG sequence, J. Magn. Reson. (1969) **79**, 28 (1988).
[26] A. M. Souza, G. A. Álvarez, and D. Suter, Robust dynamical decoupling, Phil. Trans. R. Soc. A **370**, 4748 (2012).
[27] J. F. Barry, J. M. Schloss, E. Bauch, M. J. Turner, C. A. Hart, L. M. Pham, and R. L. Walsworth, Sensitivity optimization for NV-diamond magnetometry, Rev. Mod. Phys. **92**, 015004 (2020).
[28] D. Suter and G. A. Álvarez, Colloquium: Protecting quantum information against environmental noise, Rev. Mod. Phys. **88**, 041001 (2016).
[29] L. T. Hall, C. D. Hill, J. H. Cole, and L. C. L. Hollenberg, Ultrasensitive diamond magnetometry using optimal dynamic decoupling, Phys. Rev. B **82**, 045208 (2010).
[30] L. Viola, E. Knill, and S. Lloyd, Dynamical decoupling of open quantum systems, Phys. Rev. Lett. **82**, 2417 (1999).
[31] H. Y. Carr and E. M. Purcell, Effects of diffusion on free precession in nuclear magnetic resonance experiments, Phys. Rev. **94**, 630 (1954).
[32] S. Meiboom and D. Gill, Modified spin-echo method for measuring nuclear relaxation times, Rev. Sci. Instrum. **29**, 688 (1958).
[33] C. L. Degen, F. Reinhard, and P. Cappellaro, Quantum sensing, Rev. Mod. Phys. **89**, 035002 (2017).
[34] A. M. Souza, G. A. Álvarez, and D. Suter, Robust dynamical decoupling for quantum computing and quantum memory, Phys. Rev. Lett. **106**, 240501 (2011).
[35] M. F. Pascual-Winter, R.-C. Tongning, T. Chanelière, and J.-L. Le Gouët, Spin coherence lifetime extension in Tm^{3+}:YAG through dynamical decoupling, Phys. Rev. B **86**, 184301 (2012).
[36] N. Bar-Gill, L. M. Pham, A. Jarmola, D. Budker, and R. L. Walsworth, Solid-state electronic spin coherence time approaching one second, Nat. Commun. **4**, 1743 (2013).
[37] M. Zhong, M. P. Hedges, R. L. Ahlefeldt, J. G. Bartholomew, S. E. Beavan, S. M. Wittig, J. J. Longdell, and M. J. Sellars, Optically addressable nuclear spins in a solid with a six-hour coherence time, Nature (London) **517**, 177 (2015).
[38] M. Loretz, J. M. Boss, T. Rosskopf, H. J. Mamin, D. Rugar, and C. L. Degen, Spurious harmonic response of multipulse quantum sensing sequences, Phys. Rev. X **5**, 021009 (2015).
[39] G. T. Genov, D. Schraft, and T. Halfmann, Rephasing efficiency of sequences of phased pulses in spin-echo and light-storage experiments, Phys. Rev. A **98**, 063836 (2018).
[40] T. Gullion, D. B. Baker, and M. S. Conradi, New, compensated Carr-Purcell sequences, J. Magn. Reson. (1969) **89**, 479 (1990).
[41] G. De Lange, Z. H. Wang, D. Ristè, V. V. Dobrovitski, and R. Hanson, Universal dynamical decoupling of a single solid-state spin from a spin bath, Science **330**, 60 (2010).
[42] N. Aharon, I. Cohen, F. Jelezko, and A. Retzker, Fully robust qubit in atomic and molecular three-level systems, New J. Phys. **18**, 123012 (2016).
[43] G. T. Genov, N. Aharon, F. Jelezko, and A. Retzker, Mixed dynamical decoupling, Quantum Sci. Technol. **4**, 035010 (2019).
[44] G. T. Genov, Y. Ben-Shalom, F. Jelezko, A. Retzker, and N. Bar-Gill, Efficient and robust signal sensing by sequences of adiabatic chirped pulses, Phys. Rev. Res. **2**, 033216 (2020).
[45] M. C. Wang and G. E. Uhlenbeck, On the theory of the Brownian motion II, Rev. Mod. Phys. **17**, 323 (1945).
[46] D. T. Gillespie, The mathematics of Brownian motion and Johnson noise, Am. J. Phys. **64**, 225 (1996).
[47] C. Adambukulam, B. Johnson, A. Morello, and A. Laucht, Hyperfine spectroscopy and fast, all-optical arbitrary state initialization and readout of a single, ten-level ^{73}Ge vacancy nuclear spin qudit, arXiv:2309.04126.
[48] C. T. Nguyen, D. D. Sukachev, M. K. Bhaskar, B. Machielse, D. S. Levonian, E. N. Knall, P. Stroganov, R. Riedinger, H. Park, M. Lončar, and M. D. Lukin, Quantum network nodes based on diamond qubits with an efficient nanophotonic interface, Phys. Rev. Lett. **123**, 183602 (2019).
[49] C. T. Nguyen, D. D. Sukachev, M. K. Bhaskar, B. Machielse, D. S. Levonian, E. N. Knall, P. Stroganov, C. Chia, M. J. Burek, R. Riedinger, H. Park, M. Lončar, and M. D. Lukin, An integrated nanophotonic quantum register based on silicon-vacancy spins in diamond, Phys. Rev. B **100**, 165428 (2019).
[50] S. Maity, B. Pingault, G. Joe, M. Chalupnik, D. Assumpcao, E. Cornell, L. Shao, and M. Lončar, Mechanical control of a single nuclear spin, Phys. Rev. X **12**, 011056 (2022).